Silicon Nanoparticles Produced by Femtosecond Laser Ablation in Ethanol: Size Control, Structural Characterization, and Optical Properties

ARTICLE *in* THE JOURNAL OF PHYSICAL CHEMISTRY C · AUGUST 2010

Impact Factor: 4.77 · DOI: 10.1021/jp102174y

9 AUTHORS, INCLUDING:

Serge Garnov
Russian Academy of Sciences
197 PUBLICATIONS **1,091** CITATIONS
SEE PROFILE

Cosmin Farcau
Babeş-Bolyai University
46 PUBLICATIONS **525** CITATIONS
SEE PROFILE

Robert Carles
Paul Sabatier University - Toulouse III
139 PUBLICATIONS **1,933** CITATIONS
SEE PROFILE

Valérie Guieu
University Joseph Fourier - Grenoble 1
22 PUBLICATIONS **434** CITATIONS
SEE PROFILE

Silicon Nanoparticles Produced by Femtosecond Laser Ablation in Ethanol: Size Control, Structural Characterization, and Optical Properties

Petr G. Kuzmin and Georgy A. Shafeev*

Wave Research Center of A.M. Prokhorov General Physics Institute of the Russian Academy of Sciences, 38, Vavilov Street, 119991 Moscow, Russian Federation

Vladimir V. Bukin and Sergei V. Garnov

A.M. Prokhorov General Physics Institute of the Russian Academy of Sciences, 38, Vavilov Street, 119991 Moscow, Russian Federation

Cosmin Farcau, Robert Carles, and Bénédicte Warot-Fontrose

CEMES, UPR CNRS 8011, 29, rue Jeanne Marvig, BP 94347, 31055 Toulouse Cedex 4, France

Valérie Guieu and Guillaume Viau*

Université de Toulouse, LPCNO, INSA, UMR CNRS 5215, 135 avenue de Rangueil, 31077 Toulouse Cedex 4, France

Received: March 10, 2010; Revised Manuscript Received: July 26, 2010

Spherical silicon nanoparticles were prepared by laser ablation of a single crystal Si wafer immersed in 95% ethanol with a pulse duration shorter than the time of electron−phonon relaxation (from 35 to 900 fs). The size distribution depends on the pulse duration as well as the width of the size distribution, which increases with the increase of the laser pulse duration. High resolution transmission electron microscopy performed on 20−40 nm particles showed polycrystalline particles made up mainly of silicon (α-Si) crystallites with the diamond structure and in some cases cubic silicon carbide (SiC) inclusions. Electron energy loss spectroscopy data on the large particles are very similar to bulk Si. Raman analysis extended to small frequencies showed a downshift and an asymmetrical broadening of the first-order Si optical peak with respect to bulk Si in good agreement with a spatial confinement in 5−10 nm crystallites. The photoluminescence spectra present a maximum of emission band at about 640 nm.

1. Introduction

Silicon nanocrystals present great interest in various fields of applications, in nanoelectronics as charge carriers in Si nanocrystal single-transistor memory cells[1] and photoconductive thin films[2] or in medicine as molecular oxygen sensitizers for biomedical applications.[3−5] Silicon nanoparticles are also studied in materials science as precursors for nanostructured Si−C composites as electrode materials in lithium-ion batteries.[6] While various techniques like ion implantation,[7] conventional laser ablation in ultrahigh vacuum,[8] or pulse laser deposition[9] were developed for the fabrication of Si nanoclusters, monolayers, and thin films of Si nanocrystals embedded in an oxide matrix, only very few examples of silicon colloidal solutions are found in the literature. Nevertheless, either for biomedical applications or for electronic devices elaborated by low cost integration methods, colloidal solutions of well-defined nanoparticles are desired. The wet chemistry methods, that are very useful to prepare colloidal solutions of several metals or semiconductor particles, are not so easy in the case of silicon. The chemistry of silicon often requires a high temperature process or the use of highly reducing agents. Si nanocrystals were obtained by thermal decomposition of organosilanes in supercritical hexane,[10] reduction of silicon tetrachloride with Zintl salts,[11] or sodium naphtalide.[12] More recently, reaction of sodium silicide with ammonium bromide leads to hydrogen terminated silicon nanoparticles.[13] Microcrometer size grains made up of silicon nanocrystals were obtained by electrochemical etching of Si single crystals in a hydrofluoric acid solution followed by a mechanical milling.[5]

CO_2 laser pyrolysis of silane SiH_4 is an alternative route that has proven its interest for the synthesis of silicon nanocrystals that can either be deposited in the desired substrate or dispersed in a solvent.[14−18] Laser ablation of a solid target immersed in liquids is another alternative route to chemical ways and has already proven to be an easy and useful tool to prepare highly electropositive metal nanoparticles. For example, aluminum nanoparticles were generated in ethanol via ablation of bulk Al in liquids with short laser pulses.[19] Recent papers describe the formation of silicon nanoparticles by laser ablation in water with ns[20,21] and fs pulse duration.[4] The influence of spatial modulation of the intensity profile of a femtosecond laser on the properties of NPs, generated in a liquid environment, has been reported.[22] In particular, it was found that Si NPs, generated by ablation of a bulk Si target in ethanol using a mask projection scheme, have smaller average size than those generated with a laser beam with a Gaussian intensity profile. The laser ablation in liquids is a complex process and involves a number of experimental parameters. Recent numerical modeling of laser ablation of a solid immersed into a transparent radiation liquid is based on the different Lennard-Jones potentials in the adjacent media.[23]

10.1021/jp102174y
Published on Web 08/24/2010

The model predicts that the main ablation mechanism is not due to the phase explosion in the target material.

This paper deals with multiparametric studies of silicon nanoparticles generated by laser ablation of bulk silicon in ethanol with femtosecond laser pulses at variable pulse duration. The influence of the duration of the laser pulse in the range 35−900 fs is described. This pulse duration is shorter than the time of electron−phonon relaxation in Si, which is typically of the order of a few picoseconds. One might expect that the properties of nanoparticles produced with variable femtosecond pulse duration are sensitive to the processes of electron relaxation within the Si lattice. Photoluminescence and Raman response of generated Si NPs down to shifts as low as 50 cm^{-1} are studied.

2. Experimental Section

The experimental details on nanoparticle generation by laser ablation of solids in liquid are described in detail elsewhere.[24] A single crystal Si wafer was chosen as a target. Ethanol (95%) was used as a working liquid for ablation.

Laser radiation was focused onto a target under an ethanol layer from 2 to 3 mm thick. The volume of the liquid was 10 mL for each exposure. A cell with liquid was placed on a computer-driven stage which moved the target under the laser beam. This precaution was used to avoid large crater formation on the target surface, thus, to retain beam focusing on the target during ablation.

The femtosecond laser pulses were produced by a femtosecond laser system (Spectra-Physics Spitfire Pro). The single pulse energy was 2.5 mJ, the central wavelength was 800 nm, the repetition rate was 1 kHz, and the Gaussian beam diameter was 12 mm (at the $1/e^2$ level). The minimal duration of pulses was 35 fs. In the experiments, pulse duration was varied by changing the length between the diffraction grating and corner reflector inside the compressor of the regenerative amplifier. That made it possible to obtain chirped pulses with durations between 35 fs and 1 ps. The duration of femtosecond pulses was measured by an autocorrelometer (Spectra-Physics PulseScout). In all experiments, the laser fluence on the target was kept constant at 4 J/cm^2. Respectively, the peak power of the laser radiation on the target varied from 1.1×10^{11} to 4.3×10^9 W/cm^2. The exposure time for each value of laser pulse duration was 10 min. The cell with target was displaced under the laser beam during exposure.

The Si NP morphology was characterized by transmission electron microscopy (TEM) using a JEOL JEM 1400 microscope. Size distribution was inferred from TEM image analysis. High resolution transmission microscopy (HRTEM) was performed on a JEOL JEM 2100F UHR at 200 kV equipped with a field emission electron source. Electron energy loss spectroscopy (EELS) experiments were carried out on a CM20FEG transmission electron microscope fitted with a PEELS spectrometer. The low loss peak was recorded to acquire both the zero loss and the plasmon peaks.

The silicon colloidal solutions were analyzed by transmission UV−visible spectroscopy using a Perkin-Elmer Lambda 35 spectrometer. For the Raman measurements, drops of the sample solutions were deposited on a fused quartz substrate and allowed to dry. Upon solvent evaporation, clusters of Si NPs are naturally formed due to lateral capillary forces between particles and solvent convective flow. These clusters can then easily be located under the optical microscope used to collect the Raman signals. A T64000 Horiba-Jobin Yvon spectrometer was employed to record the Raman spectra, using the 482 nm radiation of an argon ion laser for excitation. To obtain a "clean" spectrum down to frequencies below 50 cm^{-1}, we used an original setup, with the excitation beam focused on the sample at oblique incidence, while the Raman scattered light was collected in standard configuration at normal incidence relative to the sample support. Very low laser power was used (typically of 0.5 mW at the entrance of a 10× objective), to avoid heating effects, which can distort the measured spectra.

Photoluminescence spectra were acquired from the same deposited samples, by using a Dilor XY (Vis) spectrometer and a 488 nm line of an argon laser for excitation. Photoluminescence spectra were also recorded on colloidal solutions using a 400 nm excitation wavelength and a power of 5 mW.

3. Results and Discussion

Particle Shape and Size. Laser ablations of a silicon target immersed in 95% ethanol using different pulse durations in the range 35−900 fs produced spherical particles (Figure 1). The size distribution is generally broad, from a few nm to about 200 nm. With pulse durations shorter than 100 fs, an important amount of particles observed by TEM present a diameter below 3 nm (Figure 1b) and these fine particles present the tendency to self-assemble in a monolayer on the carbon membrane of the TEM grid. With longer pulse durations, a majority of spherical particles with a diameter in the range 30−100 nm were obtained (Figure 1c).

Size distributions of NPs obtained with different pulse durations are presented in Figure 2. The mean size of the NP size distribution plotted as a function of laser pulse duration shows a well-distinguished minimum at 100 fs. The full width at half-maximum of the size distribution increases with the increase of the pulse duration (Figure 2f). The median of the size distribution presents almost the same dependence on the pulse duration with smaller values for the 35 and 100 fs pulse durations (Figure 2f). The origin of this minimum is not clear. The only time parameter of this order of magnitude in the system under study is the intraband relaxation time of electrons in Si excited by laser radiation to its conduction band. Rapid effects of electronic relaxation inside the still cold Si lattice before electron−phonon coupling occurs should be taken into account in modeling, as well as viscous interaction of the molten layer with the expanding vapors of the surrounding liquid. The thickness of the molten layer of the target (after electron−phonon relaxation has occurred) is determined by the number of absorbed laser photons per unit area, that is, laser fluence. Since the fluence was kept constant (4 J/cm^2) for all pulse durations, this cannot account for the smaller average size of Si NPs obtained with short pulses. However, the smaller size may be due to their optical properties that allow efficient interaction with white-light continuum generation (see the Optical Properties section).

Structural Characterizations. HR TEM studies on 20−40 nm particles prepared with a pulse duration of 200 and 900 fs show a polycrystalline microstructure with a crystallite size in the range 5−10 nm. It is noteworthy that the lattice fringes are present until the particle surface showing that the amorphous silicon oxide is very thin. The diffraction patterns calculated from the high resolution image showed a majority of crystallites with the silicon diamond like structure clearly identified by the (111), (220), and (311) distances (Figure 3). Additional spots on the diffraction patterns corresponding to a distance of 2.5 Å were also observed on some particles (Figure 4). This distance does not correspond to the diamond like silicon but is in good agreement with the (111) distance of the cubic silicon carbide

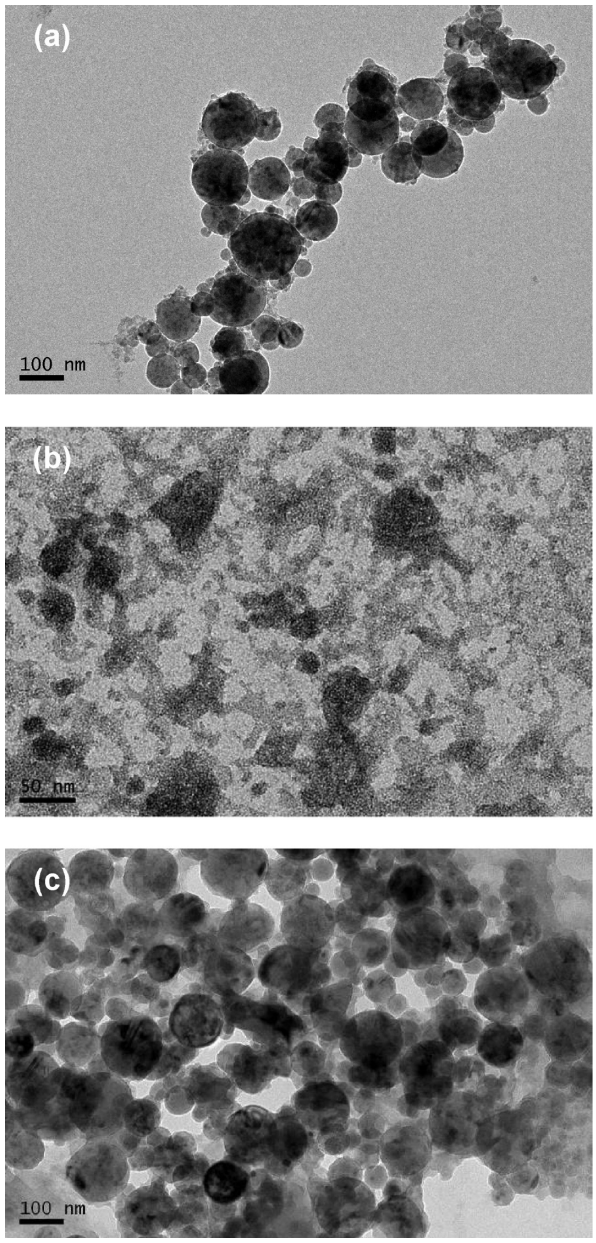

Figure 1. TEM images of Si nanoparticles prepared by ablation of a silicon target using different pulse durations: (a) 100 fs; (b) representative image of tiny particles observed with 35 fs; (c) representative image of large particles observed with 900 fs.

SiC.[25] This result is in agreement with previous observation of the dependence of the chemical composition of NPs generated by laser ablation on the nature of the liquid environment. For example, laser ablation of a Ti target in ethanol resulted in the formation of metallic Ti, while ablation of the same target in diclorethane produces NPs of TiC.[26] Also, laser ablation of Si in liquid ethanol leads to formation of SiC due to partial decomposition of ethanol to elementary carbon during the laser exposure of the target. This finding is in good agreement with observations made earlier upon laser ablation of a Si wafer in liquid ethanol.[27] The resulting colloidal solution is the mixture of both Si and SiC NPs. In that paper, some amount of aromatic hydrocarbons was added to the working liquid to increase the fraction of cubic β-SiC in the NPs generated by laser ablation in liquid ethanol with 10 ns laser pulses at a wavelength of 1.06 μm. Aromatic hydrocarbons are easily decomposed to glassy carbon upon laser exposure of a Si target immersed into them.[28] They may provide the necessary carbon species for the formation of SiC.

EELS experiments were used to differentiate between silicon, silicon oxide, or other silicon compounds. Two energy ranges in the spectrum could be used: the plasmons (collective excitation of the valence electrons) and the silicon edge (transition between occupied p and s and unoccupied states). It has been reported that the bonding modification of the Si atoms changes the energy at which the plasmon peak is measured and shifts the energy of the L edge.[29] The energy separation of the plasmons is around 6 eV between Si and SiO_2, which can be easily measured. The energy shift of the L edge between the compounds would require a better energy resolution than the one available with the apparatus. The SiC plasmon energy is too close to SiO_2 (less than 1 eV) to be distinguished with our spectrometer. Low loss spectra have been recorded on the different samples and on a SiO_2 reference to compare spectra acquired in exactly the same parameters for the microscope and the spectrometer.

Figure 5 shows the four spectra acquired on the samples using the same microscope and spectrometer settings. For the 900 fs sample (the corresponding TEM image is shown Figure 1c), the plasmon peak measured at 16 eV corresponds to the silicon; the second-order plasmon at 32 eV is also observed. The 35 fs sample (the corresponding TEM image of which is shown in Figure 1b) presents the signature of the silicon plasmon at 16 eV. A shoulder is observed on the right part of the plasmon peak that could originate from the presence of some silicon dioxide on the surface of the particles. Indeed, the EEL spectrum of standard silicon dioxide nanoparticles used as a reference presents a plasmon peak at 23 eV (Figure 5d). As expected, the proportion of oxidized silicon increases when the particle size decreases as the result of a superficial oxidation of the particles. Nevertheless, it is worth noting that even for the 2−3 nm particles the proportion of oxidized silicon remains weak. If one considers core−shell particles with a silicon core and an oxidized shell, the shell thickness corresponds to one or two monolayers.

It is well-known that Raman spectroscopy is a powerful nondestructive tool for the observation of quantum size effects in nanometer-sized particles.[30] In this size range, the Raman spectra evidence the phonon confinement effects as a downshift and a broadening of the first-order Si optical peak located around 520 cm^{-1}. Quantitative determinations of the mean size are usually achieved by a line shape analysis and using a so-called spatial confinement model (SCM).[31]

Figure 6a presents the first-order optical band for the samples made with 35 and 200 fs pulses, in comparison with that of bulk Si. For clarity, the spectrum of the 900 fs sample was not included, since the result was similar to that of the 200 fs sample. One clearly observes the Si crystalline fingerprint but with some slight downshift and asymmetrical broadening, as expected for small particles. These two correlated signatures of the reduction of the spatial correlation length are more pronounced for the 35 fs sample. Indeed, using the SCM for free-standing spherical NPs,[29,30] one deduces from the values of the downshift, 0.6 and 1.0 cm^{-1}, "Raman sizes" around 10 and 7 nm, respectively. This size is in rather good agreement with the 5−10 nm sizes of the single crystalline phases observed in TEM micrographs for the 200 fs sample (Figures 2 and 3). For the 35 fs sample, the "Raman size" is larger than the mean size observed on the TEM images. A more important shift is expected with monodisperse particles with a mean size of 2−3 nm. This discrepancy is probably due to the large standard deviation of the size

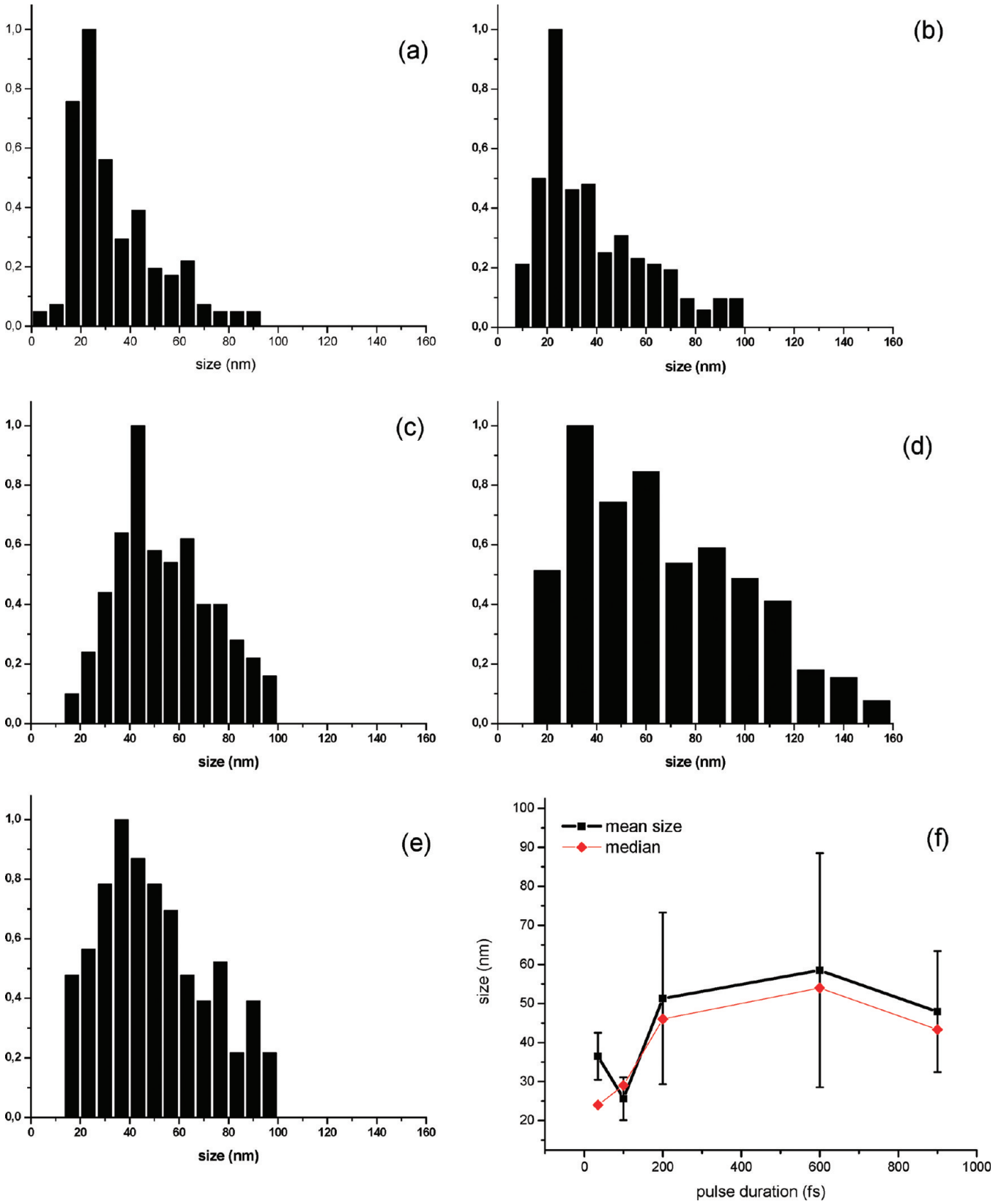

Figure 2. Size distribution calculated from TEM images of Si nanoparticles obtained by laser ablation in ethanol. Pulse duration of 35 (a), 100 (b), 200 (c), 600 (d), and 900 fs (e). Dependence on the laser pulse duration of (■) the NP mean size with the vertical bars being the full width at half-maximum of the corresponding distribution functions and (◆) NP median (f).

distribution and to the highest contribution of the largest particle to the Raman spectrum.

Moreover, in the present work, the Raman analysis is extended over an unusual wide frequency range in order to extract more information on the dynamical properties of the different deposits. We focused here only on one sample (the one produced by 35 fs pulses), with the mention that similar results were obtained for the other samples. At first (see Figure

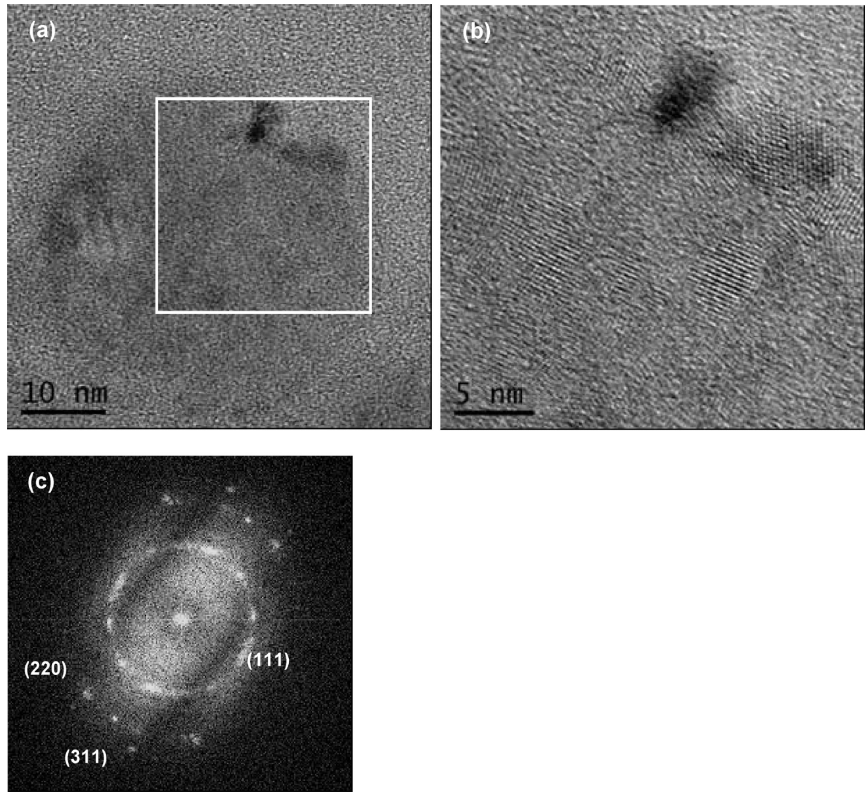

Figure 3. (a) HRTEM image of a 40 nm particle obtained with a 900 fs pulse; (b) zoom on the white square; (c) numerical diffraction pattern and spot indexation with the (111), (220), and (311) planes of α-Si.

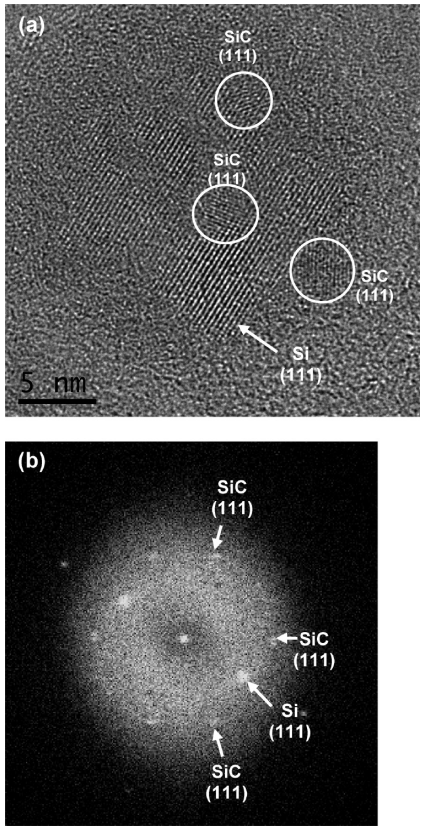

Figure 4. (a) HRTEM image of a single 20 nm particle; (b) numerical diffraction pattern and spot indexation with (111) planes of diamond like Si and (111) of cubic SiC.

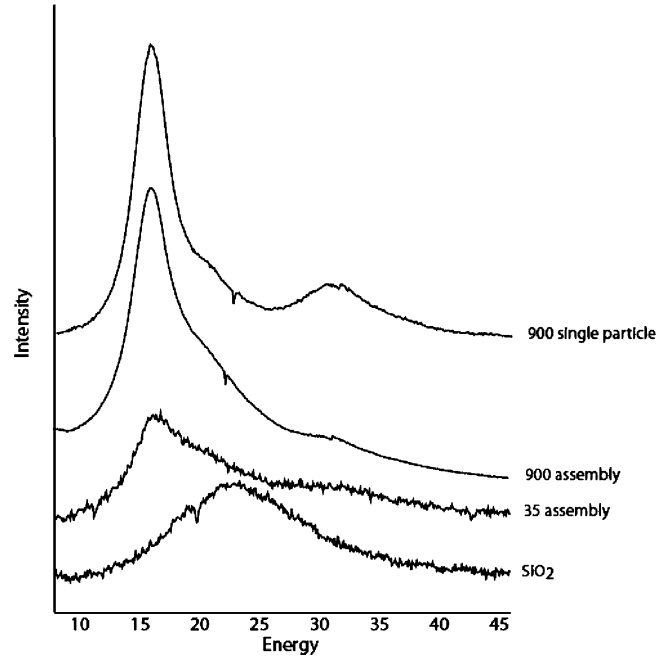

Figure 5. EELS spectra of (a) a single isolated Si 100 nm particle; (b) large area containing several 100 nm particles prepared with the 900 fs pulse duration; (c) large areas containing only 2−3 nm particles prepared by the 35 fs pulse duration; (d) SiO_2 standard particles.

6b), one observes besides the first-order long wavelength optical band, other less intense features also characteristic of crystalline Si, namely, the second-order acoustical and optical bands, centered near 300 and 960 cm^{-1}, respectively. Following the k-wave vector selection rule, they should mirror the phonon density of states with a scale multiplied by 2. Comparing with the bulk Si record, a coarsening of the Raman bands is observed but without a frequency shift: it is attributed to the decrease of long-range correlations, which wipes the sharp van Hove

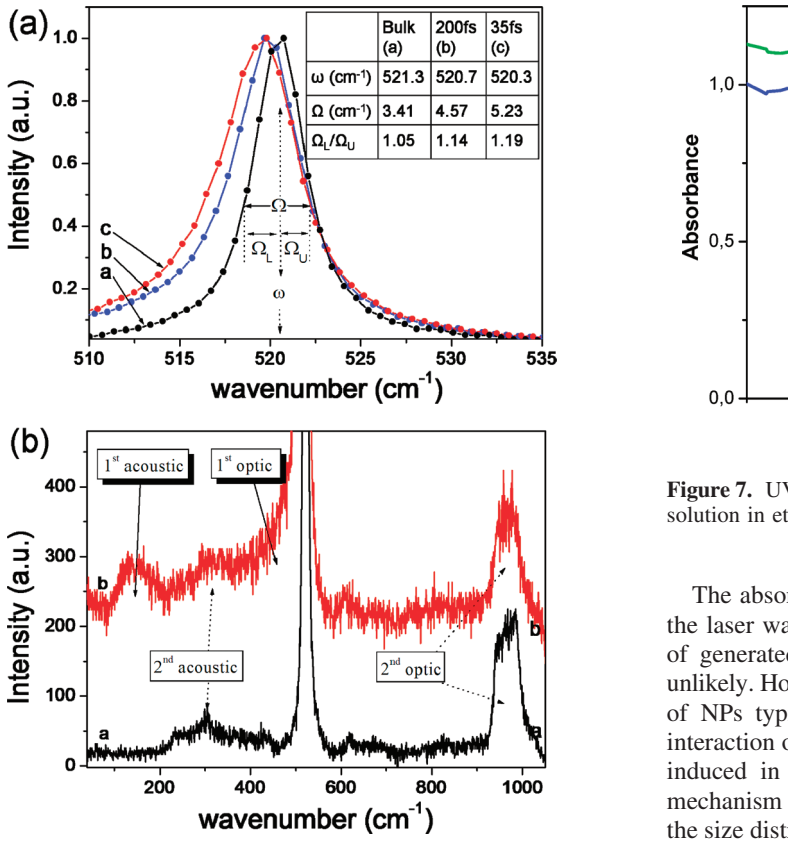

Figure 6. (a) First-order optical Raman band for the samples made with 35 fs (curve c) and 200 fs (curve b) pulses, in comparison with that of bulk Si (curve a); (b) wide-range Raman spectra of the sample prepared with 35 fs (curve b) and that of bulk Si (curve a).

singularities characteristic of a single crystal. Similar spectral features were observed previously in the Raman spectra of quantum dots of both CdS and ZnSe prepared by laser ablation of corresponding targets in liquids.[32] More interestingly, a new mode arising in the Si NP spectrum at low frequencies, with a maximum at about 150 cm^{-1}, is clearly observed. It is attributed to first-order disorder-activated transverse acoustical (DATA) scattering.[33] Such a process becomes possible when the wave vector selection rule is strongly relaxed, like in highly disordered materials. In our case, it is a clear signature of finite-size and/or disorder effects in the prepared Si NPs at a nm or sub-nm scale. It can be tentatively corroborated to TEM images that showed particles with a diameter less than 3 nm and to HRTEM images that have demonstrated the presence of disordered shells at the surface of the crystalline Si NPs and foreign crystalline phases like SiC.

Optical Properties. The colloidal solutions of Si nanoparticles in ethanol present an absorption in the UV−visible region. The maximum of absorption is about 500 nm for the 200 and 900 fs samples (Figure 7). This absorption in the visible region should be attributed to the quantum size effect on the bandgap. However, there is no visible correlation between the size and the maximum of absorption. Indeed, for the samples with a majority of 3 nm particles, the absorption is very broad and the maximum of absorption is difficult to define. The absorption in the visible region might be due to the larger Si polycrystalline particles within the samples, the population of these particles being more important with the longer pulse duration. Thus, the absorption band is certainly determined mostly by the size of nanocrystallites rather than by the general size of individual NPs.

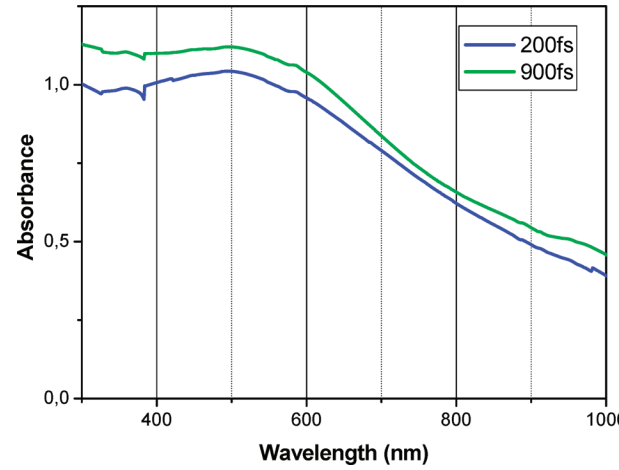

Figure 7. UV−visible absorption spectrum of Si nanoparticle colloidal solution in ethanol prepared with 200 and 900 fs pulse durations.

The absorption band of generated Si NPs is rather far from the laser wavelength of 800 nm. Therefore, the fragmentation of generated NPs due to interaction with the laser beam is unlikely. However, there is another mechanism of fragmentation of NPs typical of femtosecond laser radiation, namely, the interaction of generated NPs with so-called "white continuum" induced in the liquid by femtosecond laser radiation. This mechanism was suggested in ref 34 to explain narrowing of the size distribution of Au NPs generated by femtosecond laser ablation in water. The efficiency of generation of white continuum increases with the increase of the peak power of laser radiation and is several times higher in ethanol than in water. No systematic studies of the intensity of white continuum were done in the present work. However, qualitatively, its intensity decreases with the increase of the laser pulse duration, from maximum at 35 fs and no visible continuum at 900 fs pulse duration. Moreover, the appearance of NPs during laser exposure of the Si target enhances the intensity of white-light continuum. The spectral width of continuum in ethanol is very wide, and it fits the broad absorption peaks of Si NPs well. Therefore, the interaction of the white continuum with generated Si NPs may be the reason for their size reduction, especially at 35 fs pulse duration (see Figure 2f). Note also that excitation of the white light continuum in the liquid consumes laser photons and therefore results in lower laser fluence on the target. In general, the average size of NPs decreases with the decrease of the laser fluence on the target due to the smaller thickness of the molten layer.[35]

Photoluminescence (PL) measurements were performed on the as-prepared colloidal solutions deposited on a quartz substrate, as described for Raman experiments. All three types of samples exhibited some degree of photoemission, and interestingly at the same spectral position, around 600 nm. A representative PL spectrum of deposited Si NPs (sample prepared with 35 fs pulses) is presented in Figure 8 (curve a), showing a broad band peaking at about 610 nm. Further, we have verified if the substrate is emissive, and indeed, an emission band centered at about 575 nm was detected (curve b in Figure 8). Thus, by subtracting the substrate spectrum from the Si NPs-on-substrate spectrum, an emission band centered around 635 nm is clearly evidenced (curve c in Figure 8), and attributed to PL of Si NPs. Both the position and shape of the emission band correlate very well with the PL spectrum measured directly on the colloidal solutions (Figure 9). Some recent results[36] on luminescence from Si NPs of different sizes would indicate an

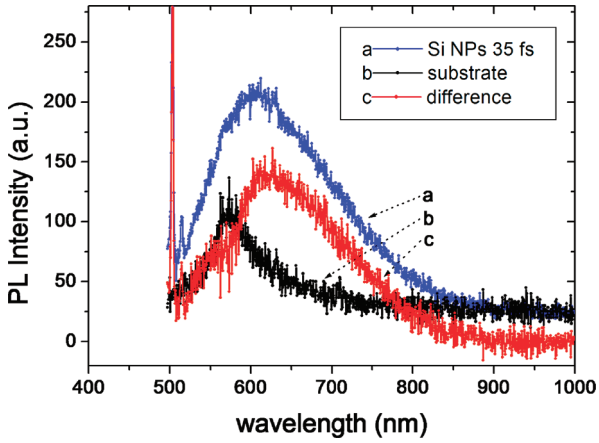

Figure 8. PL spectra of Si NPs deposited on the quartz substrate (curve a), bare quartz substrate (curve b), and Si NPs (curve c), obtained by subtraction of spectrum b from spectrum a (excitation wavelength: 488 nm).

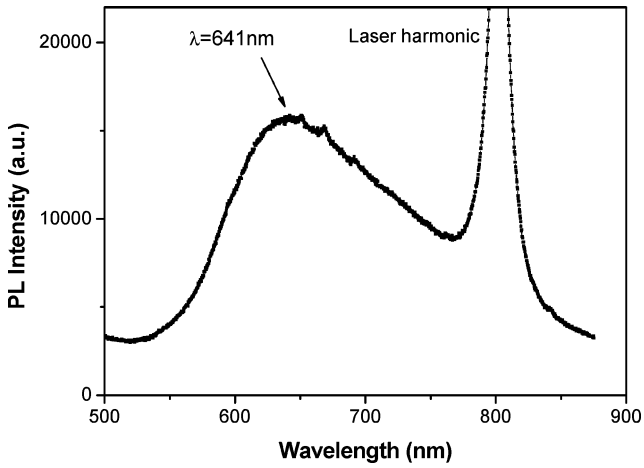

Figure 9. Photoluminescence spectrum of a colloidal solution of Si nanoparticles in ethanol prepared with a 200 fs pulse duration and a mask (excitation wavelength, 400 nm; power, 5 mW).

average size between 2 and 3 nm for an emission band like ours, located at 635 nm. This is consistent with the size of nanoparticles prepared by 35 fs pulses, as observed in TEM measurements. However, the similarity between the PL spectra of 35 and 200 fs samples (the latter being made up of crystallites with sizes between 5 and 10 nm) suggests a common origin of the PL, which is probably not due to pure size effects. More likely, the observed PL is activated by disorder or some type of surface defects, which could be inherent to the laser abaltion technique. Thus, the PL could have the same microscopic structural origin as the DATA scattering discussed in the previous section. The luminescence of the 35 fs sample is probably due to the larger particles that are difficult to isolate from the 3 nm size particles. It is noteworthy that PL in this spectral region was not reported for Si nanoparticles prepared by laser ablation in aqueous solution,[21] showing that the solvent has a strong influence on the optical properties of the particles. Actually, the emission band recorded on our particles is much more similar to the luminescence of Si nanocrystals prepared by gas phase laser pyrolysis of silane.[18]

4. Conclusion

Laser ablation of silicon in ethanol is a simple and convenient method to prepare Si nanoparticles in colloidal solution. The center of the size distributions decreases with the decrease of laser pulse duration as well as the width of the distribution. The interaction of the Si particles with the white-light continuum generated with low pulse duration may be a reason of the size reduction, as it was previously suggested in the case of gold nanoparticles.

Laser ablation of silicon in ethanol leads to poorly oxidized silicon particles as inferred from HRTEM, EELS, and Raman experiments. It was confirmed by their luminescence properties that are very different from those of the Si particles obtained by ablation in an aqueous medium. EELS shows that even the assemblies of the smallest 3 nm particles present the spectroscopic properties of silicon. This study confirmed also that ethanol is partially decomposed down to elementary carbon during the ablation process, since SiC crystallites were inferred by HRTEM. However, in pure ethanol, the proportion of SiC remains quite low because it was not detected by Raman spectroscopy.

Acknowledgment. The authors thank V. Collière (LCC, Toulouse) for TEM and HR TEM characterizations. The work was partially supported by the Russian Foundation for Basic research, Grant No. 10-02-90044.

References and Notes

(1) Shalchian, M.; Grisolia, J.; Ben Assayag, G.; Coffin, H.; Atarodi, S. M.; Claverie, A. *Appl. Phys. Lett.* **2005**, *86*, 163111.
(2) Pradhan, S.; Chen, S.; Zou, J.; Kauzlarich, S. M. *J. Phys. Chem. C* **2008**, *112*, 13292.
(3) Kovalev, D.; Gross, E.; Künzner, N.; Koch, F.; Timoshenko, V. Yu.; Fuji, M. *Phys. Rev. Lett.* **2002**, *89*, 137401.
(4) Rioux, D.; Laferrière, M.; Douplik, A.; Shah, D.; Lilge, L.; Kabashin, A. V.; Meunier, M. M. *J. Biomed. Opt.* **2009**, *14*, 021010.
(5) Timoshenko, V. Yu.; Kudryavtsev, A. A.; Osminkina, L. A.; Vorontsov, A. S.; Ryabchikov, Yu. V.; Belogorokhov, I. A.; Kovalev, D.; Kashkarov, P. K. *JETP Lett.* **2006**, *83*, 423.
(6) Saint, J.; Morcrette, M.; Larcher, D.; Laffont, L.; Beattie, S.; Pérès, J.-P.; Talaga, D.; Couzi, M.; Tarascon, J.-M. *Adv. Funct. Mater.* **2007**, *17*, 1765.
(7) Bonafos, C.; Carrada, M.; Cherkashin, N.; Coffin, H.; Chassaing, D.; Ben Assayag, G.; Claverie, A.; Müller, T.; Heinig, K. H.; Perego, M.; Fanciulli, M.; Dimitrakis, P.; Normand, P. *J. Appl. Phys.* **2004**, *95*, 5696.
(8) Patrone, L.; Nelson, D.; Safarov, V. I.; Sentis, M.; Marine, W.; Giorgio, S. *J. Appl. Phys.* **2000**, *87*, 3829.
(9) (a) Riabinina, D.; Durand, C.; Margot, J.; Chaker, M.; Botton, G. A.; Rosei, F. *Phys. Rev. B* **2006**, *74*, 075334. (b) Umezu, I.; Sugimura, A.; Makino, T.; Inada, M.; Matsumoto, K. *J. Appl. Phys.* **2008**, *103*, 024305.
(10) English, D. S.; Pell, L. E.; Yu, Z.; Barbara, P. F.; Korgel, B. A. *Nano Lett.* **2002**, *2*, 681.
(11) Bley, R. A.; Kauzlarich, S. M. *J. Am. Chem. Soc.* **1996**, *118*, 12461.
(12) (a) Baldwin, R. K.; Pettigrew, K. A.; Ratai, E.; Augustine, M. P.; Kauzlarich, S. M. *Chem. Commun.* **2002**, 1822. (b) Baldwin, R. K.; Pettigrew, K. A.; Garno, J. C.; Power, P. P.; Liu, G.-Y.; Kauzlarich, S. M. *J. Am. Chem. Soc.* **2002**, *124*, 1150.
(13) Neiner, D.; Chiu, H. W.; Kauzlarich, S. M. *J. Am. Chem. Soc.* **2006**, *128*, 11016.
(14) Khokhlov, E. M.; Kolmykov, D. V.; Kononov, N. N.; Kuzmin, G. P.; Polyakov, S. N.; Prokhorov, A. M.; Sulimov, N. A.; Tikhonevitch, O. V. *Laser Phys.* **1998**, *8*, 5.
(15) Kuzmin, G. P.; Karasev, M. E.; Khokhlov, E. M.; Kononov, N. N.; Korovin, S. B.; Plotnichenko, V. G.; Polyakov, S. N.; Pustovoy, V. I.; Tikhonevitch, O. V. *Laser Phys.* **2000**, *10*, 4.
(16) Ledoux, G.; Guillois, O.; Porterat, D.; Reynaud, C.; Huisken, F.; Kohn, B.; Paillard, V. *Phys. Rev. B* **2000**, *62*, 15943.
(17) Li, X.; He, Y.; Talukdar, S. S.; Swihart, M. T. *Langmuir* **2003**, *19*, 8490.
(18) Lacour, F.; Guillois, O.; Portier, X.; Perez, H.; Herlin, N.; Reynaud, C. *Physica E* **2007**, *38*, 11.
(19) Stratakis, E.; Barbeoroglou, M.; Fotakis, C.; Viau, G.; Garcia, C.; Shafeev, G. A. *Opt. Express* **2009**, *17*, 12650.
(20) Švrček, V.; Sasaki, T.; Shimizu, Y.; Koshizaki, N. *Appl. Phys. Lett.* **2006**, *89*, 213113.
(21) Yang, S.; Cai, W.; Zeng, H.; Li, Z. *J. Appl. Phys.* **2008**, *104*, 023516.

(22) Kuzmin, P. G.; Shafeev, G. A., Influence of intensity distribution of laser beam on the properties of nanoparticles obtained by laser ablation of solids in liquids, 2009, http://arxiv.org/abs/0907.1161.

(23) Perez, D.; Béland, L. K.; Deryng, D.; Lewis, L. J.; Meunier, M. *Phys. Rev. B* **2008**, *77*, 014108.

(24) Shafeev, G. A. Laser-based formation of nanoparticles. In *Lasers in Chemistry, Vol. 2: Influencing matter*; Lackner, M., Ed.; Wiley VCH: Weinheim, Germany, 2008; pp 713−741.

(25) JCPDS file no. 00-029-1129.

(26) Dolgaev, S. I.; Simakin, A. V.; Voronov, V. V.; Shafeev, G. A.; Bozon-Verduraz, F. *Appl. Surf. Sci.* **2002**, *186*, 546.

(27) Yang, S.; Cai, W.; Zeng, H.; Xu, X. *J. Mater. Chem.* **2009**, *19*, 7119.

(28) Simakin, A. V.; Loubnin, E. N.; Shafeev, G. A. *Appl. Phys. A: Mater. Sci. Process.* **1999**, *69*, S267–S269.

(29) Schamm, S.; Bonafos, C.; Coffin, H.; Cherkashin, N.; Carrada, M.; Ben Assayag, G.; Claverie, A.; Tencé, M.; Colliex, C. *Ultramicroscopy* **2008**, *108*, 346.

(30) Paillard, V.; Puech, P.; Laguna, M. A.; Carles, R.; Kohn, B.; Huisken, F. *J. Appl. Phys.* **1999**, *86*, 1921.

(31) Richter, H.; Wang, Z. P.; Ley, L. *Solid State Commun.* **1981**, *39*, 625.

(32) Anikin, K. V.; Melnik, N. N.; Simakin, A. V.; Shafeev, G. A.; Vitukhnovsky, A. G. *Chem. Phys. Lett.* **2002**, *366*, 357.

(33) Zwick, A.; Carles, R. *Phys. Rev. B* **1993**, *48*, 6024.

(34) Besner, S.; Kabashin, A.; Meunier, M. *Appl. Phys. A: Mater. Sci. Process.* **2007**, *88*, 269.

(35) Simakin, A. V.; Voronov, V. V.; Kirichenko, N. A.; Shafeev, G. A. *Appl. Phys. A: Mater. Sci. Process.* **2004**, *79*, 1127.

(36) Sato, K.; Tsuji, H.; Hirakuri, K.; Fukata, N.; Yamauchi, Y. *Chem. Commun.* **2009**, *25*, 3759.

JP102174Y